

# Energy minima and ordering in ferromagnets with quenched randomness

D. A. Garanin

*Physics Department, Herbert H. Lehman College and Graduate School, The City University of New York,  
250 Bedford Park Boulevard West, Bronx, New York 10468-1589, USA*

(Dated: June 9, 2025)

Energy minimization at  $T = 0$  and Monte Carlo simulations at  $T > 0$  have been performed for 2D and 3D random-field and random-anisotropy systems of up to 100 million classical spins. The main finding is that 3D random-anisotropy systems magnetically order on lowering temperature, contrary to the theoretical predictions based on the Imry-Ma argument. If random-anisotropy is stronger than the exchange, which can be the case in sintered materials, the system still orders but the magnetization is strongly reduced and there is a large spin-glass component in the spin state, the heat capacity having a cusp instead of a divergence. 3D random-field systems do not magnetically order on lowering temperature but rather freeze into the correlated spin-glass state. Here, although magnetized local energy minima have lower energies than non-magnetized ones, magnetic ordering is prevented by singularities pinned by the random field.

## I. INTRODUCTION

Quenched or static randomness is ubiquitous in solid-state physics, strongly affecting different types of ordering. In magnetic systems, randomness arises via lattice defects as well as random anisotropy, which is usually due to the amorphous or sintered structure of these materials [1, 2]. Other physical systems include flux lattices in superconductors [3–5], thin films on imperfect substrates [6], pinned charge-density waves [7], superfluid  $^3\text{He-A}$  in aerogel [8, 9], magnetic-bubble lattices [10, 11], liquid crystals [12] to name a few. Larkin, with the help of the Green's functions (GF) method, had shown that whatever weak pinning potentials destroy the long-range translational order of flux lattices [3]. The same method was applied to charge-density waves [7].

Important classes of systems with quenched randomness are systems with random field (RF) and random anisotropy (RA). For magnetic systems, the most relevant is the RA model as the crystal field produces only even combinations of the spin-vector components due to the time-reversal symmetry. In theoretical investigations, one usually uses the simplified model of spins on a regular lattice with the RA [13]. An effective random field arises in diluted antiferromagnets in the presence of an applied uniform magnetic field [14]. A random field can be used to model pinning centers in different systems. Apart from that, the RF model is important theoretically as the most basic model of static randomness in magnetic systems.

The interest in systems with quenched randomness increased after the seminal work by Imry and Ma [15], in which suppression of long-range order (LRO) in magnetic systems with continuous symmetry by whatever weak random field was suggested based on a simple energy argument. This amounts to the absence of magnetization in the ground state of these systems. Aizenman and Wehr [16, 17] provided a mathematical argument that is considered to be a rigorous proof of the Imry-Ma statement. Imry-Ma's simple approach leads to qualitatively the same results as the sophisticated GF method

by Larkin. Both yield a correlation length that is finite at  $T = 0$  and diverges in the limit of weak randomness, signaling the absence of the LRO. This is why both together are sometimes called the Larkin-Imry-Ma (LIM) argument, albeit theoretically they have little in common. So below the abbreviation IM for the Imry-Ma argument will be used.

Random-anisotropy model was investigated with the help of the mean-field theory [18], Monte Carlo [19], perturbation theory [20], and scaling [21]. Early work was summarized in Ref. [22], as well as in a much later Ref. [23], which uses the renormalization-group method. In particular, Aharony and Pytte [20], inspired by the Imry-Ma argument, stated that the RA model has zero magnetization and a huge magnetic susceptibility at low temperatures.

The GF method was applied to the classical 3D  $xy$  ferromagnetic RF model in Ref. [24] and to the 3D arbitrary-component spin-vector RF model in Refs. [25, 26], in both cases with parallel direct numerical energy minimization for spins on the lattice. This research to a significant extent was fueled by the idea to numerically check the theoretical work criticizing the Imry-Ma argument [27, 28] and proposing a power-law dependence of the correlation function based on the renormalization group with replicas [29–34] (for a review, see Ref. [35]), variational approach [36], as well as Monte Carlo simulations [37–40]. In particular, Refs. [19, 32, 33, 36–40] deal with spin systems. This hypothetical quasiordered phase, presumed to be vortex-free in spin systems and dislocation-free in flux lattices, received the name of a Bragg glass (see, for instance, Ref. [34]). In Refs. [24, 26] it was found that at short distances the spin correlation functions (CF) follow the predictions of the GF theory, and the numerically found values of the ferromagnetic correlation radius  $R_f$  coincide with those obtained by the GF method. No power-law dependences were observed at large distances,  $R \gtrsim R_f$ .

It was suggested, although never proven rigorously or demonstrated numerically on large systems, that the RA model behaves similarly to the RF model. The GF

method was applied to RA ferromagnets in Refs. [41–43] much earlier than it was applied to RF ferromagnets. Similarly to the latter and Ref. [20], it was conjectured that there is no LRO in RA ferromagnets and  $R_f$  is large for a weak RA, which implies an extreme softness (a large magnetic susceptibility) of amorphous and sintered magnets. Such a state was called a *correlated spin glass*. Magnetic hysteresis in the 3D RA ferromagnet, which is not captured by the GF method, was studied by numerical energy minimization in Ref. [44]. Freezing of the 2D RA ferromagnet into a correlated spin glass was investigated in Ref. [45] by Monte Carlo simulations, and it was inferred that the freezing mechanism is likely blocking of spin flips by anisotropy barriers rather than a true spin-glass transition.

Possible applications of RA magnets include very soft magnetic elements, as predicted in Refs. [41–43], and efficient broadband absorbers of the microwave energy [46–48]. Although at the atomic scale anisotropy relative to the exchange is small as a relativistic effect, it is largely augmented in granular materials where directions of the random-anisotropy axes are the same within grains [44, 49].

Numerical results of Refs. [24, 26, 44] uncovered another aspect of the behavior of systems with quenched randomness. Both RF and RA models possess zillions of local energy minima separated by energy barriers. As a result of energy minimization or processes on the system (lowering the temperature, sweeping the magnetic field, etc.) the system can end up in any of these states, not necessarily in the ground state. Energy minimization of the RF model starting from the random initial condition (RIC) for spins leads to the spin-glass state with nearly zero magnetization. The same starting from the collinear initial condition (CIC) leads to a partially ordered state. In this case, the spin CF decreases with  $R_f$  calculated by the GF method, but then flattens out, revealing incomplete disordering with a significant residual magnetization. If the amplitude of the RF is small enough, this state is free of singularities (vortices, vortex loops, hedgehogs), which are ignored in the GF approach, as well as in the Imry-Ma argument. In the case of RIC, there are lots of singularities that increase the energy of the system and make the magnetization vanish. Magnetic correlation radius in this case (called  $R_V$  in Ref. [24] because of vortex loops in the 3D  $xy$  model) is controlled by the concentration of singularities and is significantly smaller than  $R_f$  resulting from the GF calculation.

Singularities play a major role in the ordering/disordering of systems with quenched randomness. In the last section of Ref. [24], and then in a more general and focused form in Ref. [25], it was shown that, if the spins follow the random field averaged over the region of the linear size  $R_f$ , as assumed in the Imry-Ma argument, this inevitably leads to formation of singularities: vortices in the 2D  $xy$  model, vortex loops in the 3D  $xy$  model, hedgehogs in the 3D Heisenberg model. In the 2D Heisenberg model, there are no singularities, but there

are nonsingular topological objects – skyrmions. For the general  $n$ -component spins in  $d$  dimensions, at  $n \leq d$  the presence of singularities leads to strong metastability and glassy behavior, with the final state depending on the initial condition. At  $n = d + 1$ , when topological structures are nonsingular, the system possesses a weak metastability. At  $n > d + 1$ , when topological objects are absent, the final, lowest-energy state is independent of the initial condition. It is characterized by the exponential decay of correlations that agrees quantitatively with the theory based upon the Imry-Ma argument. One can generalize these findings, stating that any true disordering (excluding quasi-regular structures with zero magnetization, such as stripe domains) leads to the formation of singularities. The role of the latter may be preventing complete disordering of the system if the increase of the energy due to singularities dominates the energy decrease due to further aligning with the RF. Results of Refs. [24–26] indicate that all RF systems disorder except for the 3D  $xy$  model, in which the energy of creating vortex loops is very high.

So far, numerical investigations of the RA model are scarce in comparison to those of the RF model. One can name Refs. [44, 45] cited above, as well as the Monte Carlo study of a spin chain with RA [50] and small systems with RF and RA in Refs. [38, 39], despite the RA systems being more relevant for applications. This can be partially explained by the belief that RA has a similar effect to RF. However, there is an important difference – the degeneracy of the RA energy with respect to the inversion of spins. Whereas in the RF model energetically favorable directions of spins cover the whole sphere, in the RA model the directions of the spins can be reduced to a hemisphere, which minimizes the exchange energy. This is the case of the strong RA, in which the spin polarization in the ground state is  $m = 1/2$  for unit-length classical spin vectors. This differs radically from the predictions based on the Imry-Ma argument and the GF approach made for a weak RA. However, weakening RA relative to the exchange interaction is unlikely to increase disordering – one can expect the opposite. Based on the energy argument above, one can expect that RA systems will order with lowering temperature, although the equilibration can be slowed down by energy barriers, especially at low  $T$ .

The objective of this work is to clarify the question of ordering in magnetic systems with static disorder, especially in RA systems, with the help of energy minimization at  $T = 0$  and Monte Carlo simulations at finite temperatures. This requires working with large systems as the magnetic correlation radius  $R_f$  can be large, and the system size  $L$  should satisfy  $L \gg R_f$  to avoid ordering as a trivial finite-size effect. Current computing resources make it possible.

The structure of the remaining part of the paper is the following. In Sec. II the model of classical ferromagnets with RF and RA is introduced, and the theoretical background based on the Imry-Ma argument and Green's

function approach is reviewed. In Sec. III the numerical methods, the energy minimization, and the Monte Carlo with thermalized overrelaxation are explained. Section IV contains the numerical results subdivided into three groups: (i) Sampled local energy minima in RA and RF systems in 2D and 3D; (ii)  $D_R$  and  $H_R$  scans at  $T = 0$  which reveal the change of the ground state; (iii) temperature dependences of the magnetization and other physical quantities. The results are summarized in the Conclusion.

## II. THE MODEL

Consider the model of classical spins on a square or cubic lattice

$$\mathcal{H} = -\frac{1}{2} \sum_{i,j} J_{ij} \mathbf{s}_i \cdot \mathbf{s}_j - H_R \sum_i (\mathbf{n}_i \cdot \mathbf{s}_i) - \frac{D_R}{2} \sum_i (\mathbf{n}_i \cdot \mathbf{s}_i)^2 - \mathbf{H} \cdot \sum_i \mathbf{s}_i \quad (1)$$

with either RF (second term) or RA (third term) taken into account. Here  $J_{ij}$  is the coupling of the  $n$ -component spin vectors  $|\mathbf{s}_i| = 1$  with the coupling constant  $J > 0$  between the nearest neighbors,  $H_R > 0$  is the RF constant,  $D_R > 0$  is the RA constant,  $\mathbf{n}_i$  are randomly oriented unit vectors, and  $\mathbf{H}$  is the applied field in the energy units.

Before performing computations on RF and RA systems, one needs to know the magnetic correlation radius  $R_f$  to ensure it is smaller than the system's size  $L$ . The easiest way to estimate  $R_f$  is using the Imry-Ma argument. The latter in the RF case assumes that spins within a region of up to the linear size  $R_f$  are aligned with the random field averaged over this region that can be estimated as  $H_R (a/R_f)^d$ , where  $a$  is the lattice spacing and  $d$  is the dimensionality. The direction of the spins changes at the characteristic distance  $R_f$ , which costs the exchange energy via the gradient of the spin field that can be estimated as  $J (a/R_f)^2$  per spin. Both RF and exchange energies together are given by

$$E = -H_R \left( \frac{a}{R_f} \right)^{d/2} + J \left( \frac{a}{R_f} \right)^2. \quad (2)$$

where the coefficients in both terms are undefined. Minimizing  $E$  with respect to  $R_f$  yields

$$\frac{R_f}{a} = k_d \left( \frac{J}{H_R} \right)^{2/(4-d)}, \quad E = -k'_d \frac{H_R^{4/(4-d)}}{J^{d/(4-d)}}, \quad (3)$$

where  $k_d$  and  $k'_d$  are numerical factors. The result is that a ferromagnet with RF contains strongly correlated regions, which can be called *Imry-Ma domains*, although there are no boundaries between them, and thus they

can be chosen in different ways. The ferromagnetic correlation length  $R_f$  is finite for all  $d < 4$ , no matter how weak the RA is. This is usually interpreted as proof of the absence of ordering in the RF system. However, a finite  $R_f$  can exist in a partially ordered system, for instance, in the states obtained by the energy minimization from CIC (see the CF figures in Refs. [24, 26]). On the other hand, the absence of ordering is assumed in the IM construction (spins following the averaged RF). The GF calculations yield qualitatively the same results as the Imry-Ma argument. In 3D one obtains [25, 26]

$$\frac{R_f}{a} = \frac{8\pi}{1 - 1/n} \left( \frac{J}{H_R} \right)^2 \quad (4)$$

and [26]

$$E = -\frac{H_R^4}{128\pi^2 J^3}, \quad n \rightarrow \infty. \quad (5)$$

The coefficient  $k_d$  following from Eq. (4) is large but one obtains a coefficient of order one if one measures  $H_R$  against  $6J$ , which is the total exchange field from all 6 neighbors. The very small Imry-Ma adjustment energy  $E$  could be calculated analytically only for the mean spherical model,  $n \rightarrow \infty$ . In fact, the spin field is not smooth, as assumed in the IM construction, but contains a short-range component adjusting to the RF at the atomic scale  $a$ . This short-range energy in 3D is given by [26]

$$E_{\text{SR}} = -\left(1 - \frac{1}{n}\right) \frac{3H_R^2}{8\pi J}. \quad (6)$$

Because of this, it is impossible to compute the much smaller long-range energy of Eq. (5) by numerical energy minimization.

In the case of random anisotropy, the IM formulas are usually written in the same way as above with  $H_R \Rightarrow D_R$ , which leads to similar results. The argumentation becomes less transparent because the uniaxial RA becomes a general tensor after averaging over the region  $R_f$ . Although the probabilistic estimation for the components of this tensor remains valid, it is unclear how the spins follow the averaged RA. It is difficult to argue that they cover the whole sphere of the possible directions rather than a hemisphere that minimizes the exchange energy. The result for  $R_f$  obtained by the GF method for the 3D Heisenberg RA model reads [44]

$$\frac{R_f}{a} = 15\pi \left( \frac{J}{D_R} \right)^2, \quad (7)$$

where the factor 15 is close to the factor 12 for the 3D Heisenberg RF model above, Eq. (4) with  $n = 3$ . For the 2D Heisenberg model, there is only a numerical result for the magnetic correlation radius:  $R_f \simeq 11J/D_R$  [49].

Using the Imry-Ma argument, one can establish the scaling of different physical quantities such as, for instance, the microwave absorption power [49]. Instead of

performing numerical work on a system with a weak RA, which has to be big because of the large  $R_f$ , one can compute a smaller system with a stronger RA and then obtain the results for the original system with the help of the scaling. There is a more direct scaling method bypassing the IM argument. In this method, spin blocks of the size  $b$ , such as  $a \ll b \ll R_f$  are introduced [51]. Rewriting the original model on a lattice in the continuous approximation and then discretizing it again with the new lattice spacing  $b$ , one obtains the same problem in terms of a smaller number of spin blocks with a larger ratio  $D'_R/J$ , which greatly speeds up the computations. Making this scaling transformation, one obtains the dependence for  $R_f$  on the parameters which coincides with the result following from the IM argument. Here, one uses only the fact that spins are nearly aligned in the region of the linear size smaller than  $R_f$ , does not assume that the system has zero magnetization, and does not minimize its energy.

### III. NUMERICAL PROCEDURES

The numerical procedures employed here are (i) energy minimization at  $T = 0$  and (ii) Metropolis Monte Carlo at  $T > 0$ . The energy minimization combines aligning the spin  $\mathbf{s}_i$  with its effective field  $\mathbf{H}_{\text{eff},i} = -\partial\mathcal{H}/\partial\mathbf{s}_i$  with the probability  $\alpha$  and flipping the spin around the effective field,  $\mathbf{s}_i \Rightarrow 2(\mathbf{s}_i \cdot \mathbf{H}_{\text{eff},i})\mathbf{H}_{\text{eff},i}/H_{\text{eff},i}^2 - \mathbf{s}_i$  with the probability  $1 - \alpha$  (the so-called overrelaxation). The algorithm uses vectorized updates of columns of spins in checkerboard sublattices that allows parallelization of the computation. Thus, the whole (checkerboard) spin columns are either aligned with the effective field or flipped over it. This differs from the non-parallelized version in which different spins are either aligned or flipped independently, but the efficiency of both methods is comparable. For the RF model, overrelaxation is a kind of conservative pseudodynamics, which allows for better exploration of the phase space of the system. Choosing a small value of  $\alpha$  that has a meaning of the damping in this procedure (the main choice being  $\alpha = 0.03$ ) allows to achieve a much faster and deeper energy minimization than just the field alignment,  $\alpha = 1$ . For  $\alpha$  smaller than 0.03, the computation becomes longer again, but the quality of the energy minimization slightly increases (deeper local energy minima can be found). Overrelaxation is also very useful for pure systems that have a single energy minimum.

For the model with RA, overrelaxation leads to the energy decrease. It can be shown that flipping a spin changes the energy by

$$\Delta E = -\frac{D_R}{2} (\Delta \mathbf{s}_i \cdot \mathbf{n}_i)^2. \quad (8)$$

Thus, for RA, the energy minimization can be done with  $\alpha = 0$ , and there is no control over the rate of the energy decrease, such as in the RF case.

The Metropolis Monte Carlo routine for classical spin vectors includes adding a random vector to a spin and normalizing the result to obtain the trial configuration. After that, the energy change  $\Delta E$  is computed and the new spin value is accepted if  $\exp(-\Delta E/T) > \text{rand}$ , where  $\text{rand}$  is a random number in the interval  $(0, 1)$ . If  $\Delta E < 0$ , the trial is automatically accepted. Also here, updating spins is done in the vectorized and parallelized form for checkerboard sublattices. Combining Monte Carlo updates with overrelaxation greatly speeds up the thermalization. However, for RA systems (as well as for systems with coherent anisotropy) overrelaxation does not conserve the energy and it would destroy the detailed balance, which is the basis of the Monte Carlo method, leading to the energy lowering. In this case, one should use the method of *thermalized overrelaxation* [45] in which a spin is flipped around the part of  $\mathbf{H}_{\text{eff},i}$  that is independent of the given spin (i.e., the exchange and the applied field). After that, the energy change  $\Delta E$  due to the anisotropy, which can be positive or negative, is computed, and the usual acceptance/rejection criterion is applied. Note that flipping the spin over the total effective field would result in the energy lowering in all cases, and all trials will be accepted, invalidating the procedure. Thermalized overrelaxation leads to the correct thermal state, which can be checked by computing the spin temperature of the system taking into account the single-site anisotropy [52]

$$T_S = \frac{\sum_i (\mathbf{s}_i \times \mathbf{H}_{\text{eff},i})^2}{2 \sum_{i,j} J_{ij} \mathbf{s}_i \cdot \mathbf{s}_j + D_R \sum_i [3(\mathbf{n}_i \cdot \mathbf{s}_i)^2 - 1]}, \quad (9)$$

which for sufficiently large systems at equilibrium is close to the set temperature  $T$ .

For computations in a broad region of temperatures across the phase transition, it is mandatory to employ an adaptive Monte Carlo routine with an automated stopping criterion, as the number of Monte Carlo steps (MCS) necessary for equilibrating the system and measuring physical quantities changes by orders of magnitude. To monitor the equilibration, the routine uses two control quantities: the energy of the system and the magnitude  $m$  of its magnetization

$$\mathbf{m} = \frac{1}{N} \sum_{i=1}^N \mathbf{s}_i. \quad (10)$$

The MC simulation is performed in blocks of MCBlock MCS', here MCBlock = 10. After the completion of each block, the control quantities are computed. The next computational parameter is MCMass < 1 (here MCMass = 0.4), which defines the fraction of the computed data used for data processing and finally for the measurement. The routine forms the lists of the most recent data of the length  $\mathcal{L} = \text{Round}[\text{MCMass} \times N_{\text{val}}]$ , where  $N_{\text{val}}$  is the number of values of the physical quantities computed after each block. Both  $N_{\text{val}}$  and  $\mathcal{L}$  increase



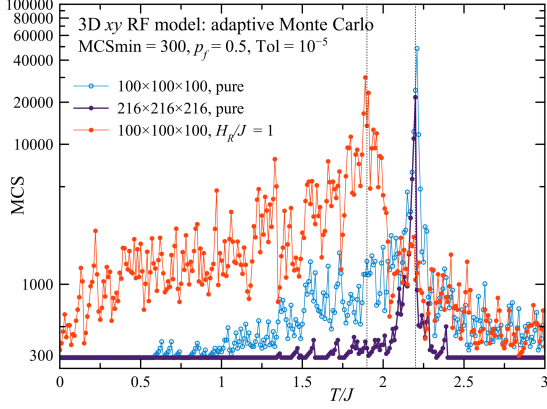


Figure 1. Adaptive Monte Carlo: MCS vs  $T$  for the 3D  $xy$  model.

in the course of the simulation. Then, for each control quantity, the routine computes the moving average over its list of length  $\mathcal{L}$  using the triangular averaging kernel  $\mathcal{K}_{\mathcal{L},j}$ :

$$Q_{\text{mean}} = \sum_{j=1}^{\mathcal{L}} \mathcal{K}_{\mathcal{L},j} Q_{\text{List}_j}, \quad \sum_{j=1}^{\mathcal{L}} \mathcal{K}_{\mathcal{L},j} = 1. \quad (11)$$

The values obtained are put into the list `QmeanList` of the same length  $\mathcal{L}$ . The triangular averaging kernel yields a rather smooth list of data, which is used to quantify the evolution of the control quantities. As  $\mathcal{K}_{\mathcal{L},j}$  has a maximum at  $j = \mathcal{L}/2$ , the values from the middle of the averaging interval  $\mathcal{L}$  make the largest contribution.

Next, the average slope of the `QmeanList` per one block is defined as

$$Q_{\text{slope}} = \frac{4}{\mathcal{L}^2} \sum_{j=1}^{\mathcal{L}} |Q_{\text{meanList}_j} - \langle Q_{\text{meanList}} \rangle|. \quad (12)$$

A sufficiently small slope could be used as the stopping criterion for the thermalization. However, for additional focusing on the regions where thermalization is slow, the routine uses the modified slope

$$\tilde{Q}_{\text{slope}} = Q_{\text{slope}} \left( \frac{\text{MCS}}{\text{MCSmin}} \right)^{p_f}, \quad (13)$$

where  $\text{MCS}$  is the total number of MCS from the beginning of the simulation and  $\text{MCSmin}$  is the minimal number of MCS required (here  $\text{MCSmin} = 300$ ). The power  $p_f$  controls the focusing: no focusing for  $p_f = 0$  and strong focusing for  $p_f = 0.5$  (here 0.35 and 0.5). One can say that focusing effectively decreases the tolerance  $\text{Tol}$  if the equilibration is slow. The stopping criterion for the equilibration reads

$$\tilde{Q}_{\text{slope}} < Q_0 \times \text{MCBlock} \times \text{Tol}, \quad (14)$$

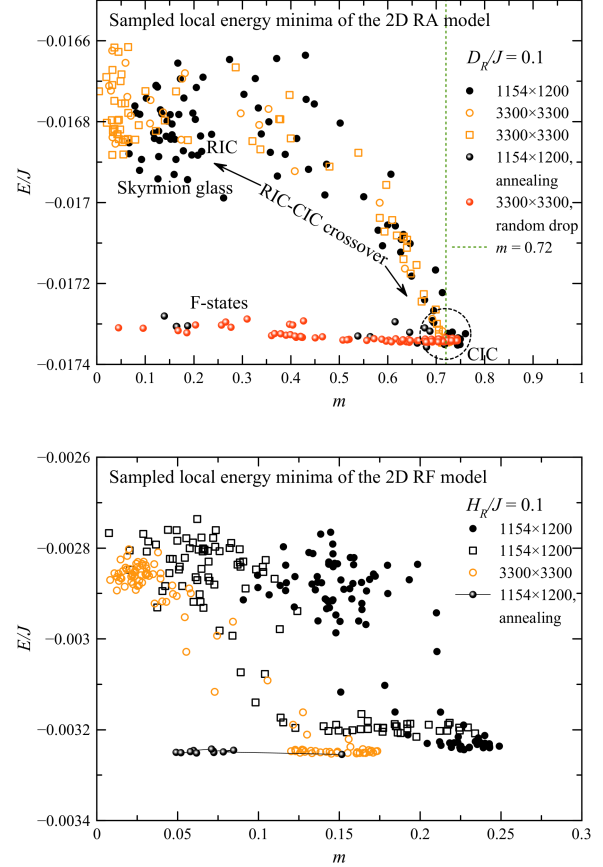


Figure 2. Local energy minima of 2D models with quenched randomness sampled by the RIC-CIC crossover, random dropping, and simulated annealing. Upper panel: 2D RA model. Lower panel: 2D RF model.

where  $Q_0$  is the characteristic value of the quantity  $Q$  ( $J$  for the energy and 1 for the magnetization) and  $\text{Tol}$  is the tolerance, here mostly  $\text{Tol} = 10^{-5}$ . For stopping, this criterion should be fulfilled for all control quantities, and  $\text{MCS}$  should exceed  $\text{MCSmin}$ . The final values of the control quantities and all other physical quantities are obtained via averaging of the most recent portion of the data of length  $\mathcal{L}$  with the averaging kernel  $\mathcal{K}$ , as in Eq. (11). In this approach, thermalization and measurement are not separated.

Computations were performed with Wolfram Mathematica in the vectorized, parallelized, and compiled form on different workstations with 16-24 processor cores and 32-64 GB of memory. The maximal system size is  $10^8$  spins for 2D and 3D systems.

Figure 1 illustrates the adaptive Monte Carlo method for the 3D  $xy$  model, computed with  $\text{MCSmin} = 300$ ,  $p_f = 0.5$ , and  $\text{Tol} = 10^{-5}$ . The number of MSC done before stopping reaches its maximum at the phase transition point: the Curie temperature  $T/J = 2.2$  in the pure model and the correlated spin-glass transition temperature  $T/J = 1.9$  for  $H_R/J = 1$ . For the larger system

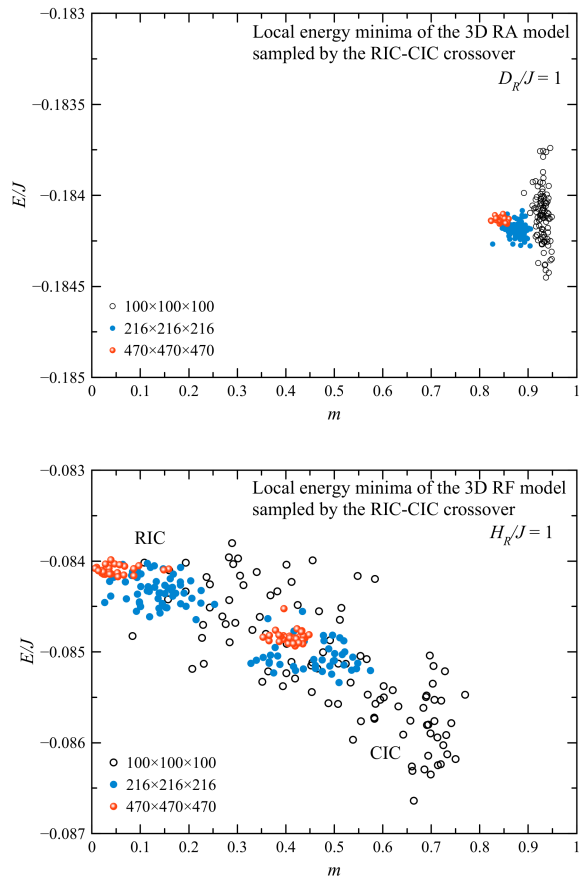


Figure 3. Local energy minima of 3D models with quenched randomness sampled by the RIC-CIC crossover. Upper panel: 3D RA model. Lower panel: 3D RF model. States on the left with lower magnetization and higher energies contain singularities (hedgehogs).

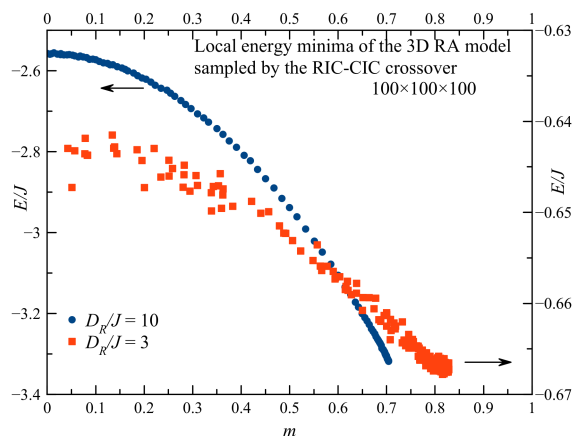


Figure 4. Local energy minima of 3D models with quenched randomness sampled by the RIC-CIC crossover:  $D_R/J = 3$  and 10. Energy minima with smaller magnetization and higher energy contain singularities (hedgehogs).

of  $216 \times 216 \times 216$  spins,  $MCS = MCS_{min}$  far from the transition point, whereas for the smaller pure system of  $100 \times 100 \times 100$  spins  $MCS > MCS_{min}$  in this region because of stronger fluctuations in smaller systems. In the glassy system with  $H_R/J = 1$ , equilibration is more difficult and requires more MCS. However, in these systems, the equilibrium is not well defined at low temperatures and cannot be reached in numerical experiments.

## IV. NUMERICAL RESULTS

### A. RIC-CIC crossover and other methods of sampling local energy minima

Large random-field and random-anisotropy systems have a huge number of local energy minima. Although it is difficult to find the ground state and enumerate all the local energy minima, one can get an idea of the energy minima by sampling them. There are several methods of sampling, one of them being the RIC-CIC crossover. Here, the energy minimization at  $T = 0$  is performed starting from the combined initial condition

$$\mathbf{s}_{initial} = \text{Normalize}[(1 - \xi) \mathbf{s}_{RIC} + \xi \mathbf{s}_{CIC}], \quad (15)$$

where  $\mathbf{s}_{initial}$  is a tensor containing all spins in the system,  $\mathbf{s}_{RIC}$  is that with randomly directed spins,  $\mathbf{s}_{CIC}$  is that with collinear spins,  $0 < \xi < 1$  is a mixing parameter, and the result of mixing the RIC and CIC states is normalized by one on each lattice site. For  $\xi$  close to zero, there is a greater possibility that the resulting state is rich in singularities or other topological structures and has a small magnetization. For  $\xi$  close to one, the resulting state should have fewer or no singularities and a larger magnetization. Energy minimization was performed for many values of  $\xi$  with different realizations of the RA.

Other methods of sampling local energy minima are so-called *simulated annealing* and *random dropping*. Both methods sample energy minima with significant magnetization and lower energy, the so-called F-states [24, 26]. Simulated annealing is a numerical experiment in which the magnetic field  $H$  is swept back and forth at  $T = 0$  with a decreasing amplitude. The values of the energy and magnetization are recorded at all points where  $H = 0$ . The random-dropping experiment consists of first minimizing the energy at  $T = 0$  with the magnetic field  $H$  applied in a random direction and then switching the field off and minimizing the energy again (dropping). The value of  $H$  is chosen to be significant but still far from saturation.

Local energy minima of a 2D 3-component RA model sampled by the RIC-CIC crossover, random dropping, and simulated annealing are shown in the upper panel of Fig. 2. The skyrmion glass [53, 54] obtained for  $\xi \ll 1$  has a higher energy and smaller magnetization than the F-states, which have their lowest energy near  $m \simeq 0.72$ , obtained with  $\xi \simeq 1$ . Random-dropping and

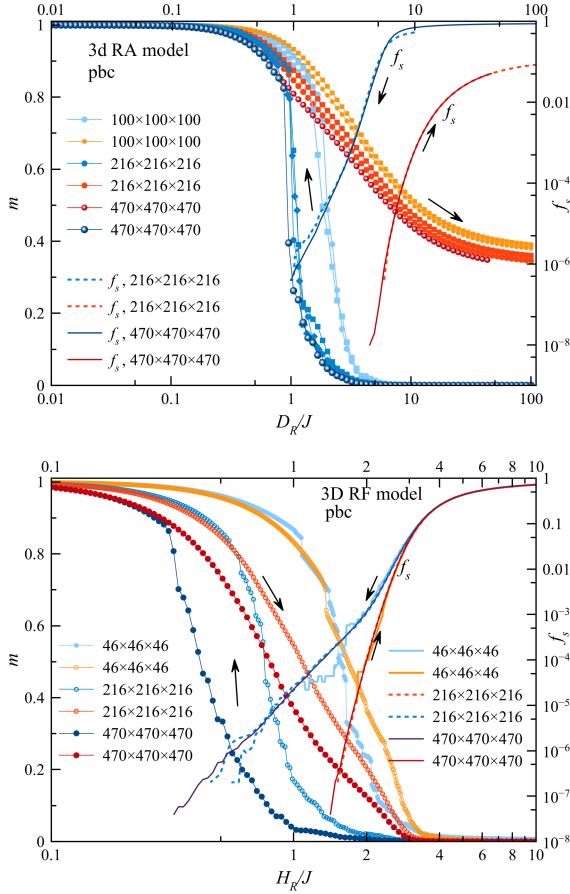


Figure 5.  $D_R$  and  $H_R$  scans with energy minimization of 3D Heisenberg systems at  $T = 0$ . Upper panel: RA model. Lower panel: RF model.

simulated annealing experiments yield a broader manifold of F-states with lower magnetization and slightly higher energy (red and black balls in the figure). This can be explained by the bending of the magnetized state, which, over large distances, can significantly reduce the magnetization while only slightly increasing the energy. These results indicate that the 2D RA model has an ordered ground state, contrary to the predictions based on the IM argument. However, this system does not order on lowering the temperature. One of the reasons is that skyrmions present at elevated temperatures do not disappear with lowering  $T$  because they are topologically protected and pinned by the RA. Also, the exchange connectivity of a 2D system with a continuous symmetry is insufficient for ordering. Results similar to those in Fig. 2 are shown in Fig. 16 of Ref. [24] for the 3D  $xy$  RF system.

The lower panel of Fig. 2 shows the sampled local energy minima of the 2D RF model. The difference is that in the RA model, the ground state has a large magnetization and does not depend on the system size, whereas in the RF model, the magnetization in the ground state is small and decreases with the system size. One can

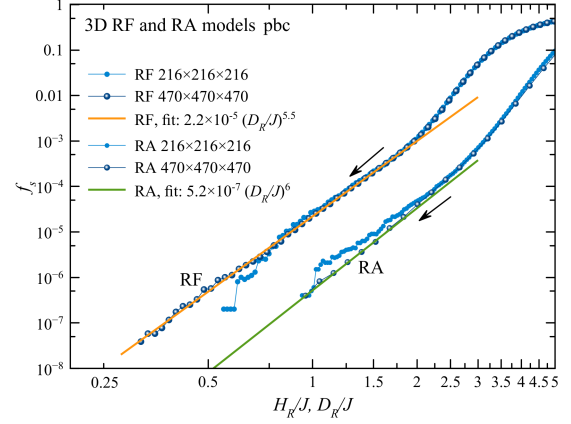


Figure 6. Concentration of hedgehogs in the 3D Heisenberg RA and RF models on lowering  $D_R$  and  $H_R$ .

expect its vanishing in the large-system limit.

Local energy minima of 3D Heisenberg RF and RA models for  $D_R/J = 1$  and  $H_R/J = 1$ , sampled by the RIC-CIC crossover method, are shown in Fig. 3. For the RA model (upper panel of Fig. 3), energy minimization ends up in the states with a large magnetization and no singularities independently of the initial condition. Increasing the system size lowers the magnetization in the ground state only insignificantly. This is a clear demonstration of a strong ordering tendency in the 3D RA model, contrary to the usually made statement that the RA destroys the ordered state in this case. For larger  $D_R/J$ , the distribution of the local energy minima is broader because there are states with singularities having smaller magnetization and larger energy, which are obtained by the energy minimization starting from the states closer to RIC. The results for  $D_R/J = 3$  and 10 are shown in Fig. 4.

In the case of the RF model (lower panel of Fig. 3), the states with higher magnetization have lower energy, although the magnetization is smaller than for the RA model and decreases with the system size. These states originate from the energy minimization starting from the initial states close to CIC and have no singularities. The states with smaller magnetization originate from the initial states close to RIC, and they have singularities (hedgehogs or Bloch points [55, 56] for the 3D Heisenberg model) that increase their energy. The role of singularities will be investigated in the next section.

## B. $D_R$ and $H_R$ scans at $T = 0$

The second type of numerical experiments performed here is  $D_R$  and  $H_R$  scans on the systems with the same RA or RF realization, with the energy minimization at  $T = 0$ . The values of  $D_R$  and  $H_R$  are increased or decreased by a small amount each time, so that the initial

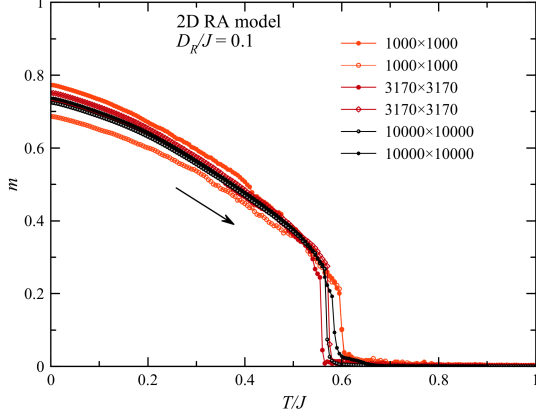


Figure 7. The (increasing) temperature dependence of the magnetization in the 2D RA model.

state of the system is already close to its final state and the energy minimization is fast. The dependences of the magnetization  $m$  and other quantities are different for increasing and decreasing the strength of RA or RF, as can be seen in Fig. 5. When the strength of the RA or RF increases (red curves), the magnetization starts at  $m = 1$  for small  $D_R/J$  or  $H_R/J$  on the left side of the figures, then it decreases because of the progressive disordering. For the RA model, this ends up in a partial disordering at large  $D_R/J$ , which is roughly consistent with the spins directed within a hemisphere,  $m = 1/2$ . In fact, the disordering is somewhat stronger with  $m$  going down to  $m \simeq 0.3$ , which means the system is not exactly in its ground state (the hemisphere distribution of spins) in the limit  $D_R \rightarrow \infty$ , which is an effect of this particular kind of evolution. For the RF model, the magnetization vanishes in the limit  $H_R \rightarrow \infty$ , as expected.

In this experiment, the concentration of singularities (hedgehogs)  $f_S$  was also computed. In the absence of a topological formula, the sum of 8 spins surrounding the center of each unit cell was computed. If the average of these 8 spins had a magnitude smaller than 0.5, a hedgehog was detected. The concentration of hedgehogs was computed as the number of hedgehogs divided by the number of cells in the system. On increasing  $D_R$  or  $H_R$ , there are no singularities at the beginning, but they emerge at critical values of  $D_R$  or  $H_R$ , then  $f_S$  grows quickly.

On decreasing  $D_R$  or  $H_R$  from large values to zero, there are lots of singularities at the beginning, and, accordingly,  $m$  is close to zero. With decreasing  $D_R$  or  $H_R$ , the exchange suppresses more and more singularities which eventually leads to nonzero values of  $m$ . In Fig. 5, one can see a clear correlation between the concentration of singularities and the magnetization. In both models, when  $f_S = 0$  is reached,  $m$  strongly increases and then continues to increase smoothly as  $D_R$  or  $H_R$  are further lowered. The difference between the two models is

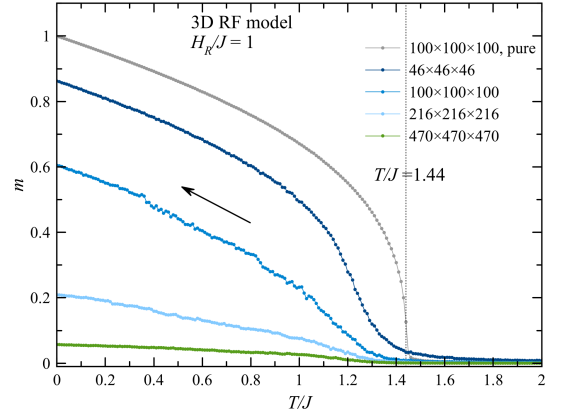
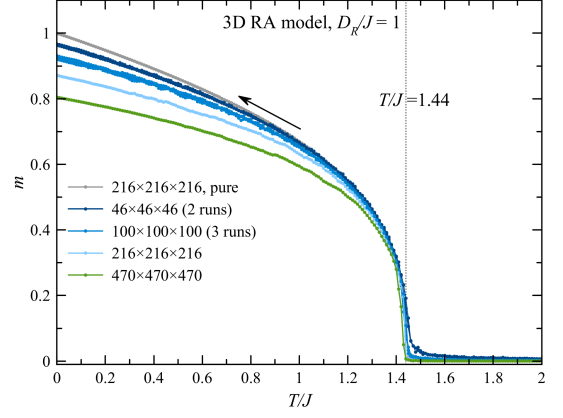


Figure 8. Temperature dependences of the magnetization of the 3D Heisenberg model with RA and RF obtained on lowering  $T$ . Upper panel: RA model. Lower panel: RF model.

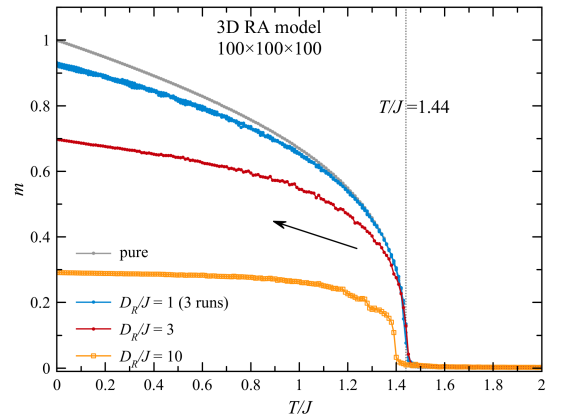


Figure 9. Temperature dependences of the magnetization of the 3D RA Heisenberg model with different values of the RA strength  $D_R$ .



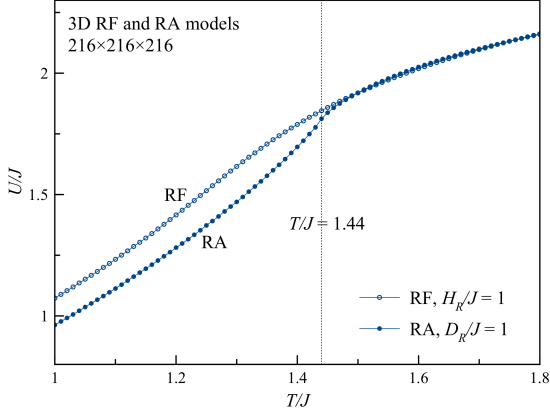


Figure 10. Temperature dependence of the energy of the 3D RA and RF models.

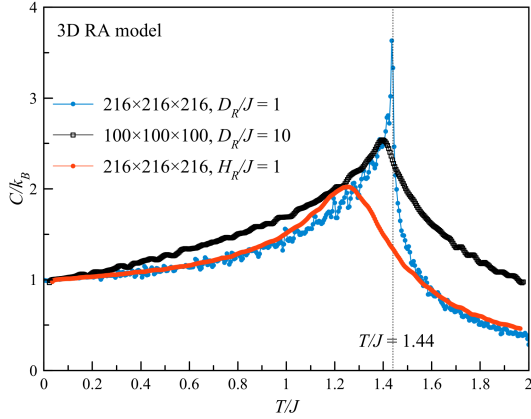


Figure 11. Temperature dependences of the heat capacity of the 3D RA and RF models.

that in the case of RA the critical value of  $D_R$  at which  $f_s$  vanishes becomes independent of the system size at large sizes such as  $216^3 \simeq 10^7$  spins and as  $470^3 \simeq 10^8$  spins, whereas in the RF case singularities turn out to be more resilient and disappear at lower  $H_R$  for larger system size. That is, for the RA, there exists a well-defined critical value of  $D_R/J$  below which singularities cannot be supported and are suppressed by the exchange. For the RF, it appears that singularities exist for whatever small values of  $H_R$  and their disappearance in systems of finite size is due to a too small concentration of singularities. Accordingly, the magnetization curves in the lower panel of Fig. 5 shift to the left with the increase of the system size.

The dependence of the concentration of singularities on the lowered  $D_R$  and  $H_R$  is shown in the separate Fig. 6. Whereas for the RA model,  $f_s = 0$  is reached at  $D_R/J \simeq 1$  for both system sizes, for the RF model there are many more singularities with no well-defined critical value of  $H_R$  at which they disappear.

Applying the topological argument of Refs. [24, 25] to the RA model, one can relate singularities and magnetic ordering. Any fully random configuration of  $n$ -component spins in  $d$  dimensions contains singularities if  $n \leq d$ . Particularly for the 3D Heisenberg model ( $n = 3$ ) there are 2D subspaces with  $s_x = 0$ ,  $s_y = 0$ , and  $s_z = 0$ . All three subspaces cross at some points where all three components of the spin field are zero. This means there are singularities at these points. Spin configurations containing singularities have zero magnetization in the limit of a large system size. If for  $n \leq d$  there are no singularities in the system, disordering of spins is not complete, and there is a nonzero magnetization for large system sizes. This is the case for the 3D RA model for  $D_R/J \leq 1$  where the singularities are suppressed by the strong exchange.

One can perform a similar investigation of 2D RA and RF models. One result is Fig. 3 of Ref. [49] for the 2D RA model obtained by the energy minimization from the CIC for all values of  $D_R/J$ . This result has an interesting and so far unexplained feature – a nearly constant value of the magnetization  $m \simeq 0.715$  in a broad interval of  $D_R/J$ , which is followed by a decrease starting at  $D_R/J \simeq 6$ . A systematic investigation of the  $D_R$  and  $H_R$  scans for 2D models is not performed here to save space.

### C. Temperature dependences

Finally, the temperature dependences of the physical quantities were computed. The 2D RA model was investigated in Ref. [45]. On lowering the temperature, this system of a sufficiently large size does not order. The question was whether it freezes into a correlated spin glass. It was found that on lowering the temperature, spins stop rotating because of blocking by the energy barriers created by the RA rather than by spin-glass freezing as a many-body effect. The heat capacity of this system has a rounded maximum without a cusp characteristic for spin glasses. Here, the question of the thermal stability of the 2D RA system prepared in the ordered state is investigated. It is well known that in the pure 2D Heisenberg ferromagnet, magnetic order is destroyed by thermal fluctuations. Monte Carlo simulations give the magnetization  $m(T)$ , which steadily decreases with the system size, and there is no well-defined transition temperature. How stable is the magnetized state of the 2D RA model at nonzero temperatures? The results of the Monte Carlo simulations using the Metropolis sampling combined with the thermalized overrelaxation are shown in Fig. 7. At the beginning, the energy was minimized at  $T = 0$  starting with CIC, then the temperature was increased in small steps, and the Monte Carlo equilibration was performed. Fig. 7 shows that the magnetized state is thermally stable. There are differences in the  $m(T)$  curves due to different realizations of the RA, but they decrease with the system's size. The magneti-

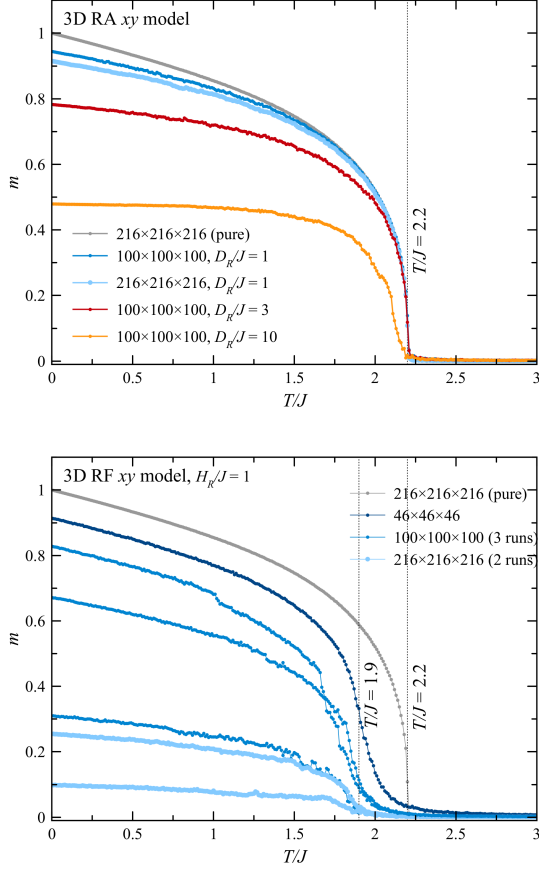


Figure 12. Temperature dependence of the magnetization of the 3D  $xy$  RA and RF models. Upper panel: RA model. Lower panel: RF model.

zation decreases with the temperature and then disappears in a jump. This behavior can be explained by the blocking mechanism. There are correlated regions, the Imry-Ma domains, pinned in the magnetized state by the anisotropy barriers. With increasing  $T$ , the magnetization in the IM domains decreases, which is seen in the figure. Finally, collective spins of the correlated regions unblock and start flipping over the barriers, which leads to the demagnetized state,  $m = 0$ . The sharp unblocking transition is the result of the automatic stopping criterion for the Monte Carlo simulation. As soon as  $m$  starts to decrease faster in the course of the simulation, the routine makes more steps to ensure equilibration, see Fig. 1. This leads to the observed jump to the demagnetized state. If a fixed number of MCS is done at each temperature, the dependence  $m(T)$  is smoother. The temperature dependence of the system's energy  $U(T)$  does not show any singularity at the unblocking point – there is only a region with a larger slope that leads to a broad maximum of the heat capacity. Such a behavior is similar to that of a system of noninteracting magnetic particles with random directions of the uniaxial anisotropy axes. Although there is exchange interaction between IM do-

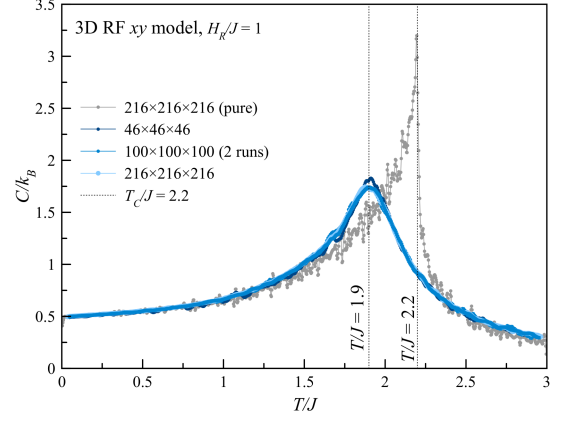


Figure 13. Temperature dependence of the heat capacity of the 3D  $xy$  RF model, compared with that of the pure system.

main, it is weak because for small  $D_R/J$  IM domains are large and the exchange connectivity in 2D is insufficient to produce many-body effects such as spin-glass freezing.

The temperature dependence of the magnetization in 3D RA and RF models was computed on lowering the temperature to check whether these systems order spontaneously. Figure 8 shows that the 3D RA systems order on lowering  $T$ , while 3D RF models order only as a finite-size effect, and ordering disappears in the limit of large systems. Also for the RA model, the magnetization at low  $T$  is decreasing with increasing system size. However, the magnetization decrease is small. Also, one should keep in mind that equilibrating a very large system, especially in the presence of energy barriers, is difficult and may take an exorbitant computing time. In real systems, there are many kinds of weak interactions that affect ordering at large distances. For instance, ferromagnets in the presence of the dipole-dipole interactions form domains that reduce the magnetization of the system. However, one does not say these materials do not ferromagnetically order. To judge about ordering, one also needs to look at the singularities at the transition point. In Fig. 8 one can see that there is a clear singularity of  $m(T)$  in the RA model similar to that for the pure system, and the phase transition temperature  $T_C/J = 1.44$  is not changed by the moderate RA such as  $D_R/J = 1$ . To the contrary, the transition in the RF model is rounded, resembling the pure ferromagnet in the applied field. Figure 9 shows that in the RA model, ordering occurs even for the strong RA such as  $D_R/J = 3$  and 10. Here, one cannot say that the magnetization at low temperatures might be a finite-size effect because for the strong RA, the magnetic correlation radius  $R_f$  is not large.

Absence and presence of the phase transition on temperature can also be seen in the comparison plot of the energies of the RA and RF models in Fig. 10. The function  $U(T)$  for the RA model has the form usual for

second-order phase transitions with a suppression just below  $T_C$ . On the other hand, for the RF model,  $U(T)$  has no pronounced features at any temperature. The heat capacity of the 3D RA and RF models obtained by differentiating  $U(T)$  is shown in Fig. 11. For the moderate-strength RA,  $D_R/J = 1$ , one has  $C(T)$  diverging at the transition point, similarly to the pure system. However, for the strong RA,  $D_R/J = 10$ , the heat capacity has a cusp typical to the spin-glass transition. In this case, the system partially orders, see Fig. 9, so one can say it has combined properties of a ferromagnet and spin glass. The RF model with  $H_R/J = 1$  also shows a maximum of  $C(T)$  at  $T/J = 1.25$  in the form of a rounded cusp.

Finally, temperature dependences of physical quantities were also computed for the 3D RA and RF two-component ( $xy$ ) spin model. The results are qualitatively similar to those of the Heisenberg model. The temperature dependences of the magnetization on lowering temperature in Fig. 12 are similar to those in Figs. 8 and 9. Note the large scatter of the data at low  $T$  for the RF  $xy$  model, caused by different realizations of the RF. Figure 13 shows the heat capacity  $C(T)$  of the 3D RF  $xy$  model compared to that of the pure system. Whereas in the pure system  $C(T)$  diverges at the Curie point  $T_C/J = 2.2$ , the system with  $H_R/J = 1$  shows a cusp at an apparent spin-glass freezing point  $T_F/J = 1.9$ .

## V. CONCLUSION

Extensive numerical experiments, including the energy minimization at  $T = 0$  and Monte Carlo at  $T > 0$  on random-field and random-anisotropy systems in 2D and 3D with 2 and 3 spin components were performed. The results show that the lowest-energy states of these systems have a significant magnetization, which contradicts the statements made in the literature about the completely disordered ground states. In RF systems, local energy levels are widely distributed, and higher-energy states with lower magnetization contain singularities that are responsible for the energy increase. On the other hand, a magnetized ground state does not automatically lead to ordering with lowering temperature because of pinned singularities.

The absence of ordering is expected in 2D systems hav-

ing global continuous symmetry. Moreover, it was shown here that the 2D RA system behaves similarly to the assembly of non-interacting magnetic particles with randomly directed uniaxial anisotropy axes. This is in agreement with Ref. [45], where blocking was observed instead of a spin-glass freezing.

In 3D RF systems, ordering is prevented by the energy barriers and pinned singularities. Instead of magnetic ordering, these systems freeze into the correlated spin-glass state. The heat capacity of these systems has a characteristic form with a cusp at the freezing temperature.

On the other hand, the 3D RA model with a moderate-strength RA,  $D_R/J \leq 1$ , has local energy levels localized in the region with a high magnetization, and these energy levels result from the energy minimization from any initial conditions. A strong preference for the magnetized states can be explained by the anisotropy of a spin having two opposite lowest-energy states that makes the ordering of spins within a hemisphere preferable in the case of the strong RA (for a weaker RA, the tendency to ordering should be even stronger). In addition, for the moderate-to-weak RA, singularities do not survive at  $T = 0$  because the exchange suppresses them. As a result, 3D RA systems order on lowering the temperature. For weak and moderate RA, relative to the exchange, the magnetic transition is similar to that in the pure system, although a thorough investigation of the critical behavior is needed. For a strong RA, the systems still order, but the magnetization is substantially reduced, and there is a considerable glassy component in this partially ordered state. The critical behavior in this case is different, having the heat capacity with a cusp instead of a divergence at the transition temperature.

In real materials, the anisotropy at the atomic scale is weak in comparison to the exchange. However, materials composed of grains with the same direction of RA within the grain have a much stronger effective RA. The computations performed above for the atomic-scale RA can be done for these materials as well.

## ACKNOWLEDGMENT

This work has been supported by the PSC-CUNY grant TRADA-54-119.

- 
- [1] P. Marín and A. Hernando, *Journal of Magnetism and Magnetic Materials* **215-216**, 729 (2000).
  - [2] O. V. Billoni, S. A. Cannas, and F. A. Tamarit, *Phys. Rev. B* **72**, 104407 (2005).
  - [3] A. I. Larkin, *Sov. Phys. JETP* **31**, 784 (1970).
  - [4] E. M. Chudnovsky, *Phys. Rev. B* **40**, 11355 (1989).
  - [5] G. Blatter, M. V. Feigel'man, V. B. Geshkenbein, A. I. Larkin, and V. M. Vinokur, *Rev. Mod. Phys.* **66**, 1125 (1994).
  - [6] E. M. Chudnovsky, *Phys. Rev. B* **33**, 245 (1986).
  - [7] K. B. Efetov and A. I. Larkin, *Sov. Phys. JETP* **45**, 1236 (1977).
  - [8] G. Volovik, *J. Low. Temp. Phys.* **150**, 453 (2008).
  - [9] J. I. Li, J. Pollanen, A. M. Zimmerman, C. A. Collett, W. J. Gannon, and W. P. Halperin, *Nature Physics* **9**, 775 (2013).
  - [10] R. Seshadri and R. M. Westervelt, *Phys. Rev. B* **46**, 5142 (1992).

- [11] R. Seshadri and R. M. Westervelt, *Phys. Rev. B* **46**, 5150 (1992).
- [12] T. Bellini, N. A. Clark, V. Degiorgio, F. Mantegazza, and G. Natale, *Phys. Rev. E* **57**, 2996 (1998).
- [13] R. Harris, M. Plischke, and M. J. Zuckermann, *Phys. Rev. Lett.* **31**, 160 (1973).
- [14] S. Fishman and A. Aharony, *Journal of Physics C: Solid State Physics* **12**, L729 (1979).
- [15] Y. Imry and S.-k. Ma, *Phys. Rev. Lett.* **35**, 1399 (1975).
- [16] M. Aizenman and J. Wehr, *Phys. Rev. Lett.* **62**, 2503 (1989).
- [17] M. Aizenman and J. Wehr, *Commun.Math. Phys.* **130**, 489 (1990).
- [18] E. Callen, Y. J. Liu, and J. R. Cullen, *Phys. Rev. B* **16**, 263 (1977).
- [19] C. Jayaprakash and S. Kirkpatrick, *Phys. Rev. B* **21**, 4072 (1980).
- [20] A. Aharony and E. Pytte, *Phys. Rev. Lett.* **45**, 1583 (1980).
- [21] A. Aharony and E. Pytte, *Phys. Rev. B* **27**, 5872 (1983).
- [22] A. Aharony, *Journal of Magnetism and Magnetic Materials* **31-34**, 1432 (1983).
- [23] M. Dudka, R. Folk, and Y. Holovatch, *Journal of Magnetism and Magnetic Materials* **294**, 305 (2005).
- [24] D. A. Garanin, E. M. Chudnovsky, and T. C. Proctor, *Phys. Rev. B* **88**, 224418 (2013).
- [25] T. C. Proctor, D. A. Garanin, and E. M. Chudnovsky, *Phys. Rev. Lett.* **112**, 097201 (2014).
- [26] D. A. Garanin and E. M. Chudnovsky, *Eur. Phys. J. B* **88**, 81 (2015).
- [27] J. L. Cardy and S. Ostlund, *Phys. Rev. B* **25**, 6899 (1982).
- [28] J. Villain and J. Fernandez, *Z. Physik B* **54**, 139 (1984).
- [29] S. E. Korshunov, *Phys. Rev. B* **48**, 3969 (1993).
- [30] T. Giamarchi and P. Le Doussal, *Phys. Rev. Lett.* **72**, 1530 (1994).
- [31] T. Giamarchi and P. Le Doussal, *Phys. Rev. B* **52**, 1242 (1995).
- [32] D. E. Feldman, *Phys. Rev. B* **61**, 382 (2000).
- [33] D. E. Feldman, *International Journal of Modern Physics B* **15**, 2945 (2001).
- [34] P. Le Doussal, *Phys. Rev. Lett.* **96**, 235702 (2006).
- [35] T. Nattermann and S. Scheidl, *Advances in Physics* **49**, 607 (2000).
- [36] T. Garel, G. Iori, and H. Orland, *Phys. Rev. B* **53**, R2941 (1996).
- [37] M. J. P. Gingras and D. A. Huse, *Phys. Rev. B* **53**, 15193 (1996).
- [38] R. Fisch, *Phys. Rev. B* **58**, 5684 (1998).
- [39] R. Fisch, *Phys. Rev. B* **62**, 361 (2000).
- [40] M. Itakura, *Phys. Rev. B* **68**, 100405 (2003).
- [41] E. M. Chudnovsky and R. A. Serota, *Phys. Rev. B* **26**, 2697 (1982).
- [42] E. M. Chudnovsky, W. M. Saslow, and R. A. Serota, *Phys. Rev. B* **33**, 251 (1986).
- [43] E. M. Chudnovsky, *Phys. Rev. B* **33**, 2021 (1986).
- [44] T. Proctor, E. Chudnovsky, and D. Garanin, *Journal of Magnetism and Magnetic Materials* **384**, 181 (2015).
- [45] D. A. Garanin and E. M. Chudnovsky, *Journal of Physics: Condensed Matter* **34**, 285801 (2022).
- [46] D. A. Garanin and E. M. Chudnovsky, *Phys. Rev. B* **103**, 214414 (2021).
- [47] D. A. Garanin and E. M. Chudnovsky, *Phys. Rev. B* **105**, 064402 (2022).
- [48] E. M. Chudnovsky and D. A. Garanin, *Phys. Rev. B* **107**, 224413 (2023).
- [49] E. M. Chudnovsky and D. A. Garanin, *Phys. Rev. B* **109**, 054429 (2024).
- [50] R. Dickman and E. M. Chudnovsky, *Phys. Rev. B* **44**, 4397 (1991).
- [51] D. A. Garanin and E. M. Chudnovsky, *Europhysics Letters* **148**, 26001 (2024).
- [52] D. A. Garanin, *Phys. Rev. E* **104**, 055306 (2021).
- [53] E. M. Chudnovsky and D. A. Garanin, *Phys. Rev. Lett.* **121**, 017201 (2018).
- [54] E. M. Chudnovsky and D. A. Garanin, *New Journal of Physics* **20**, 033006 (2018).
- [55] W. Döring, *Journal of Applied Physics* **39**, 1006 (1968).
- [56] V. M. Kuchkin, A. Haller, S. Liščák, M. P. Adams, V. Rai, E. P. Sinaga, A. Michels, and T. L. Schmidt, *Phys. Rev. Res.* **7**, 013195 (2025).